Dill, R., Klemann, V., Dobslaw, H. (2018): Relocation of River Storage From Global Hydrological Models to Georeferenced River Channels for Improved Load-Induced Surface Displacements. - *Journal of Geophysical Research*, *123*, 8, pp. 7151—7164.

DOI: http://doi.org/10.1029/2018JB016141

Journal of Geophysical Research: Solid Earth

RESEARCH ARTICLE
10.1029/2018JB016141

Relocation of River Storage From Global Hydrological Models to Georeferenced River Channels for Improved Load-Induced Surface Displacements

R. Dill[1], V. Klemann[1], and H. Dobslaw[1]

[1]Section 1.3: Earth System Modelling, Helmholtz Centre Potsdam-GFZ German Research Centre for Geosciences, Potsdam, Germany

Key Points:
- The relocation procedure maps river storage from the 0.5 degrees model representation onto a 0.125 degrees river map
- After applying the relocation procedure to modeled river storage data, the estimated hydrology-induced surface displacements significantly improve
- The relocation function can be generated automatically from the model river network

Correspondence to:
R. Dill,
dill@gfz-potsdam.de

Citation:
Dill, R., Klemann, V., & Dobslaw, H. (2018). Relocation of river storage from global hydrological models to georeferenced river channels for improved load-induced surface displacements. *Journal of Geophysical Research: Solid Earth*, *123*, 7151–7164. https://doi.org/10.1029/2018JB016141

Received 25 MAY 2018
Accepted 2 AUG 2018
Accepted article online 14 AUG 2018
Published online 30 AUG 2018

Abstract

Variations in terrestrial surface water storage cause elastic crustal displacements of several millimeters in the vertical direction on daily to seasonal time scales. Locally, strong signals with exceptionally high amplitudes can be observed along the major river channels. As the horizontal resolution of global hydrological models is typically limited to 0.5° × 0.5°, the generalized model drainage network leads to simulated river mass distributions that are not necessarily collocated with the real courses of the rivers. Moreover, the spreading of locally concentrated surface water on the coarse model grids leads to substantially underestimated amplitudes of simulated hydrologically induced surface displacements. We therefore develop a relocation procedure to improve such hydrological loading estimates, especially at locations near the river banks. We separate the water masses stored in the modeled river network from the total water storage and relocate them on a georeferenced river map with higher resolution. Applying the relocated river masses, simulated hydrological loading amplitudes increase by 0.2–5 mm for the vertical load-induced surface displacement along the major rivers, at the Amazon even up to additional 15 mm. The amplitudes for the horizontal load-induced surface displacements are slightly increased, up to maximum 3 mm. Besides changes in the distance to the mass loads, the horizontal displacement fields is also heavily affected by significant changes in the directions to the relocated river mass load. The comparison of modeled hydrologically induced surface displacement time series with Global Positioning System observations shows a significantly improved fit for stations in close proximity to larger rivers when applying the relocation procedure.

Plain Language Summary Variations in terrestrial surface water loads cause an elastic deformation of the Earth's lithosphere of several millimeters in the vertical direction. Locally, strong signals with exceptionally high amplitudes can be observed along the channels of large river like the Amazon, Nile, or Lena. In order to predict such hydrology-induced surface displacements, mass distributions from global hydrological models are employed. Due to the limited resolution of such modeled mass loads, typically only 0.5°, the outspread and dislocated river mass distributions lead underestimated displacement amplitudes at even wrong locations. We therefore develop a relocation procedure to improve such hydrological loading estimates, especially at locations near the river banks. Water stored in model's river network is mapped onto a georeferenced river map with higher spatial resolution. Simulated hydrological loading amplitudes calculated from the refined river storage estimates significantly improve along the world's major rivers when compared to displacement time series as observed with Global Positioning System.

1. Introduction

The elastic response of the Earth's lithosphere to variations in the terrestrially stored water can reach amplitudes that exceed contributions from nontidal atmospheric surface pressure variations. Particularly along the major river channels, exceptionally high amplitudes in the radial component of geodetic station coordinate time series can be found (Fu et al., 2012). In the Amazon Basin near the main river channel, Bevis (2005) related the seasonal signal of 50 to 75 mm in the up component of the GPS (Global Positioning System) measurement at Manaus to the loading effect of water masses stored in the Amazon and Rio Negro stream channels. In

addition to the dominant seasonal water mass variations in surface water compartments like rivers and lakes, episodic heavy rain events cause regional to local river storage maxima that lead to subseasonal hydrologically induced displacements. Such location specific signals can be found at many stations in the coordinate time series of GPS (Jiang et al., 2013; Williams & Penna, 2011) and Very Large Baseline Interferometry (Petrov & Boy, 2004) observations.

In order to interpret or correct geodetically observed station coordinates for hydrological loading effects, sufficiently accurate load-induced displacement predictions from numerical models are necessary. In principle, a higher resolution for the mass load distribution leads to a more detailed result for the surface displacement. In the temporal domain, monthly averages might be sufficient to represent most of the predominantly seasonal signal of hydrological loading. In the spatial domain, however, the hydrology-induced displacement fields reveal small-scale features due to the strong heterogeneity in water mass distribution in particular along the major rivers. Here the mass distribution has to be represented in great detail. Typically, loading estimates based on global hydrological models rely on mass distributions given on 1.0° or 0.5° regular grids (e.g., Fritsche et al., 2012; Rajner & Liwosz, 2011). Loading calculations based on mass variation taken from satellite missions as realized with GRACE (Gravity Recovery And Climate Experiment, 2002–2017; e.g., Collilieux et al., 2011; Tregoning et al., 2009) and GRACE-FO (launched in May 2018) suffer from even much coarser spatial resolutions. Dill and Dobslaw (2013) demonstrated the influence of using different resolutions for the water mass load and for the representation global-gridded surface displacements. They concluded that globally gridded hydrological loading results should be made available at least at the same spatial resolution as the mass load is provided by a global hydrological model, for example, 0.5°. Even displacement patterns derived for mass loads with small-scale features given on a 0.125° grid could be well represented on the 0.5° global grid, since the stiffness of the Earth lithosphere effectively acts as a low-pass filter in the spatial domain. Increasing further the resolution for the mass load would require also higher resolutions for the data sets of hydrological loading accompanied with a substantial growth in computational costs and storage capacities. By keeping the conventional 0.5° resolution for the gridded hydrological loading, the results can be improved by increasing the spatial resolution of the hydrological mass distribution up to 0.125°. The spatial scale of mass loads influences also the sensitivity of the elastic deformation response to shallow crustal heterogeneities. High-resolution mass loads in combination with local Green's Functions considering local crustal structures instead of a single global Green's Function can lead to differences in the hydrological loading estimates of up to ± 1 mm in both radial and horizontal directions (Dill et al., 2015).

This study presents our approach to enhance the spatial resolution of simulated water masses in the model river flow compartment from a model-based 0.5° grid to a georeferenced 0.125° grid (see Figure 1). The relocation procedure relates each river grid cell of the hydrological model to their matching georeferenced river grid cells extracted from high-resolution river courses based on Geo Information System data, as described in section 2. In order to test the influence on hydrological loading estimates, we apply the relocation procedure to surface water masses of the river compartment from the global hydrological model LSDM (Land Surface Discharge Model; Dill, 2008). Subsequently, we calculate in section 3 hydrology-induced surface displacements by means of a patched Green's Function approach as introduced in Dill and Dobslaw (2013) that is able to handle globally such highly heterogeneous mass distributions. In section 4, we compare the hydrology-induced surface displacements based on the refined river mass distribution with reference results based on the original model mass distribution and quantify the improvements by evaluating the model predictions to observed station coordinate time series followed by some conclusions in section 5.

2. Relocation of River Water

Global grid-based hydrological models require a detailed definition of the local drainage and discharge directions. A direction map connects each grid cell with one of its eight neighboring grid cells. Together, all drainage directions represent the model river network. Such direction maps are typically derived from a raster digital elevation model following the lowest topography value downstream to the ocean. To improve the drainage structure over flat areas, information on the location of major rivers is implemented by the so-called stream burning method proposed by Maidment (1996) and refined later by Wesseling et al. (1997). High-quality river maps are available from HydroSHED (Hydrological Data and Maps Based on Shuttle Elevation Derivatives at Multiple Scales; Lehner et al., 2006) with resolutions of 30″ or even 15″ which corresponds to 0.9 or even 0.45 km. As global hydrological models are defined on much coarser resolutions, one has to

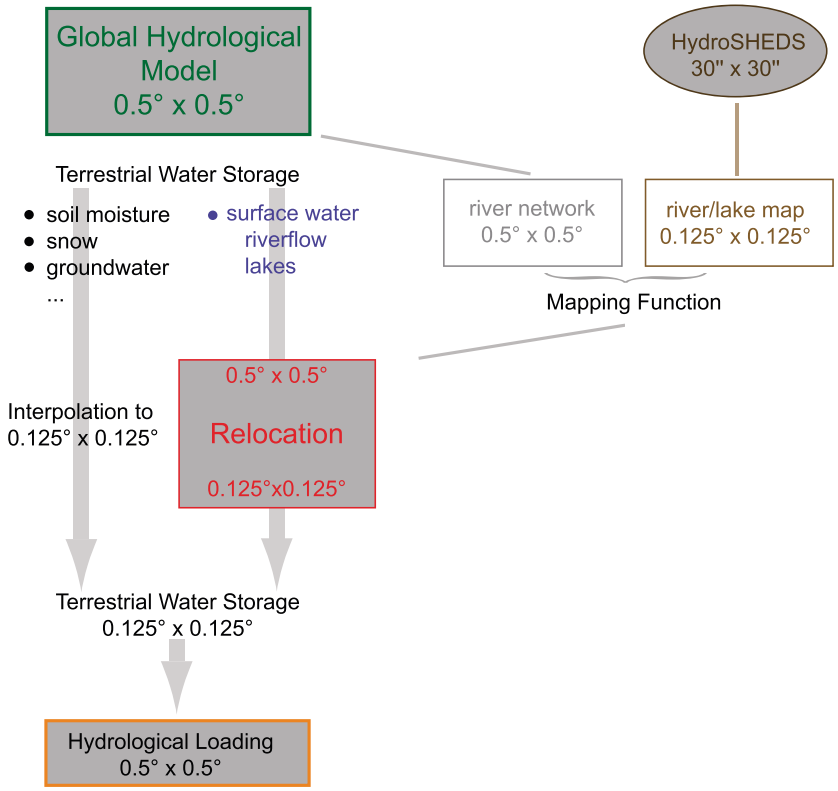

Figure 1. Flow chart of the relocation procedure to map surface water masses extracted from a 0.5° global hydrological model river network into a 0.125° river map prior to the calculation of hydrology-induced surface displacement.

aggregate the information from the high-resolution HydroSHED grid into grid cells of 1.0° or 0.5°. For global hydrological models, this generalization process is typically done under the objective to conserve the catchment areas and river length in order to easily implement the parametrizations of physical processes like surface mass balance or discharge velocity. Artifacts like shifted locations of river channels or river nodes into neighboring grid cells are accepted in order to keep the major river sections and their drainage directions separated. In consequence we have to deal with two uncertainty sources when considering the water mass distribution in the modeled river compartment. First, like all other storage compartments, the river masses in the models are spread homogeneously over the whole area of the model grid cells and second, with wrong geographic locations.

In case of the LSDM 0.5° model river network, the grid cell centers can deviate from the location of the real river channel by more than 75 km. In the worst case, geodetic stations located near the river might even appear on the opposite bank when projected to the model grid. In order to improve the modeled river mass distribution, a new 0.125° map of river and lake locations is derived from the 30″ HydroSHED data set by applying the technique of grid cell aggregation. The 0.125° river map is much less affected by generalization errors than the model 0.5° river network, and the grid cell centers of the major rivers follow much better the geographic river channels.

The main challenge is to project the water masses stored in the 0.5° model river network $M_{0.5}$ into the new georeferenced 0.125° river map $G_{0.125}$ without destroying the model hydrograph, that is, the temporal evolution of the water transport. Figure 2 displays the deviations between $M_{0.5}$ (black arrows and gray shades) and $G_{0.125}$ (orange shades). As the length of river sections, that is, the cumulative distance between grid cell centers, deviates between $M_{0.5}$ and $G_{0.125}$ it is not possible to simply project the water mass stored in each 0.5° grid cell into a fixed number of 0.125° grid cells. Instead, we follow an approach developed by Kisseler (2010) and quantify how far each 0.125° grid cell belongs to a certain 0.5° grid cell. These 259, 200×4, 147, 200 matching weights are defined by

$$W_{mg} = a \cdot c \cdot \left[F^D \cdot (1-d) + F^N \cdot d\right] \cdot (1-u) \cdot (1-l) \quad (1)$$

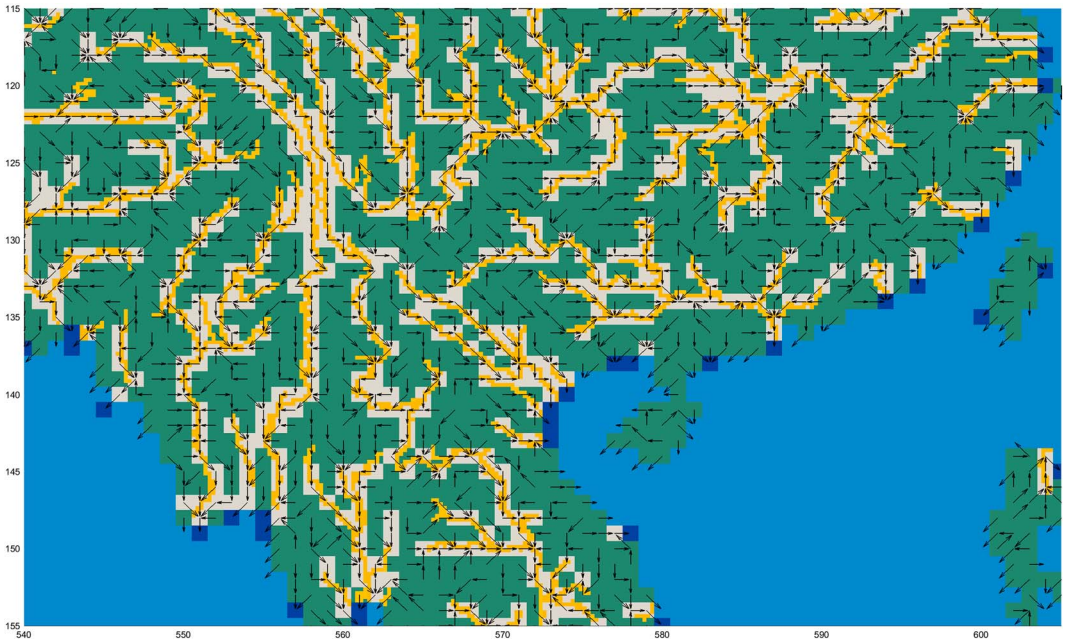

Figure 2. Comparison between 0.5° model river network (black arrows, beige grid cells) and 0.125° georeferenced river map (orange grid cells). Map shows the Yunnan province in southwest China, axis give the regular 0.5° grid cell 720 × 360 indices. For better readability only grid cells with higher accumulation values indicating bigger rivers are displayed. All grid cells with lower accumulation values are left green.

for all grid cells $m \in M_{0.5}$ and $g \in G_{0.125}$. The two flags a and c are set only for associated pairs of grid cells according to

$$a = \begin{cases} 1, & (A_m^c - A_g^c)/A_m^c < 1 \\ 0, & \text{otherwise} \end{cases} \tag{2}$$

$$c = \begin{cases} 1, & (P_m^c - P_g^c) < 3° \\ 0, & \text{otherwise} \end{cases} \tag{3}$$

Here the main characteristics to identify pairs of grid cells in $M_{0.5}$ and $G_{0.125}$ that represent the same part of a river are the normalized upstream catchment area, A_m^c and A_g^c, and the geographic catchment center, P_m^c and P_g^c. The upstream catchment areas are calculated from the accumulation value multiplied by the grid cell area, where the accumulation value counts the number of upstream grid cells. The catchment centers are defined as geographic center of all counted upstream grid cells.

In order to downweight the matching of associated grid cells with increasing distance D between the grid cell center locations, P_m^l and P_g^l, we define an empirically adjusted distance factor F_D

$$F^D = \begin{cases} 1/3\,(2 - D/r), & D \le r \\ 1/6\,(3 - D/r), & r < D < 3r \\ 0, & 3r \le D \end{cases} \tag{4}$$

where $r = 0.5°/\sqrt{2}$ is the model grid cell half diameter. Further grid cell characteristics have to be taken into account to avoid the distribution of water masses from the main river course into tributaries with similar catchment characteristics A^c and P^c in the region of river nodes. The flags d and u

$$d = \begin{cases} 1, & \text{g inside any } m' \text{ downstream of } m \\ 0, & \text{otherwise} \end{cases} \tag{5}$$

$$u = \begin{cases} 1, & \text{g inside any } m' \text{ upstream of } m \\ 0, & \text{otherwise} \end{cases} \tag{6}$$

are set if the 0.125° grid cell g is located inside any downstream or upstream 0.5° grid cell m′ of the considered 0.5° grid cell m, respectively. In case the 0.125° grid cell is located inside the 0.5° downstream part

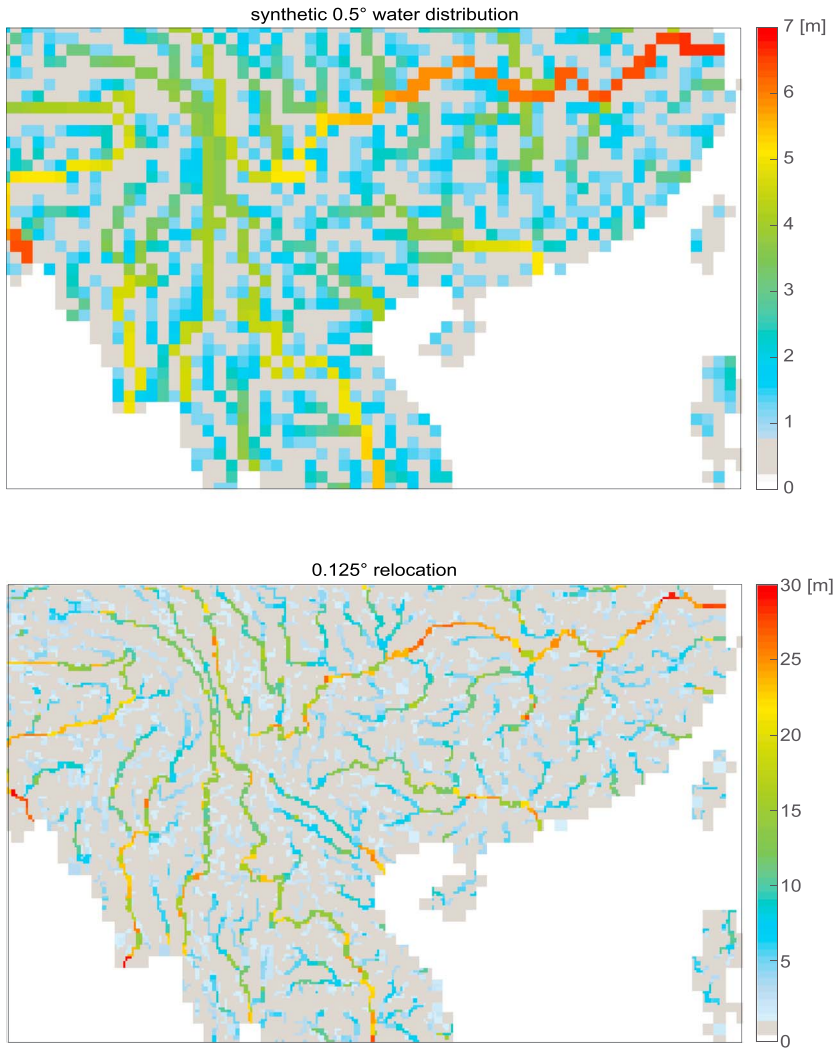

Figure 3. (top) Synthetic 0.5° water distribution for the Land Surface Discharge Model river network in the Yunnan province in southwest China. (bottom) 0.125° water distribution after applying the newly developed river relocation method.

($d = 1$) nearby the next river node P_m^N, we switch from the distance-depending factor F^D to a constant factor F^N defined as

$$F^N = \begin{cases} 2/3, & N \le r \\ 0, & \text{otherwise} \end{cases} \tag{7}$$

where $N = P_g^l - P_m^N$ is the distance from the 0.125° grid cell center to the next 0.5° node. We also exclude grid cells marked in the model as lakes ($l = 1$), because their mass will be distributed homogeneously into the related 0.125° lake area in a separate step.

After evaluating all W_{mg} for each pair of $m \in M_{0.5}$ and $g \in G_{0.125}$, we rearrange and normalize W_{mg} according to

$$R_{mg} = \frac{W_{mg}}{\sum_g W_{mg}} \tag{8}$$

The relocation function R_{mg} gives the partitioning of each hydrological mass h_m stored in a 0.5° grid cell into its associated 0.125° grid cells. Finally, we obtain the refined mass distribution h_g from

$$h_g = R_{mg}\, h_m \tag{9}$$

Factors in equations (4) and (7) as well as the thresholds in equations (2) and (3) were determined empirically by checking the plausibility of the relocation function with a synthetic mass distribution for the LSDM river

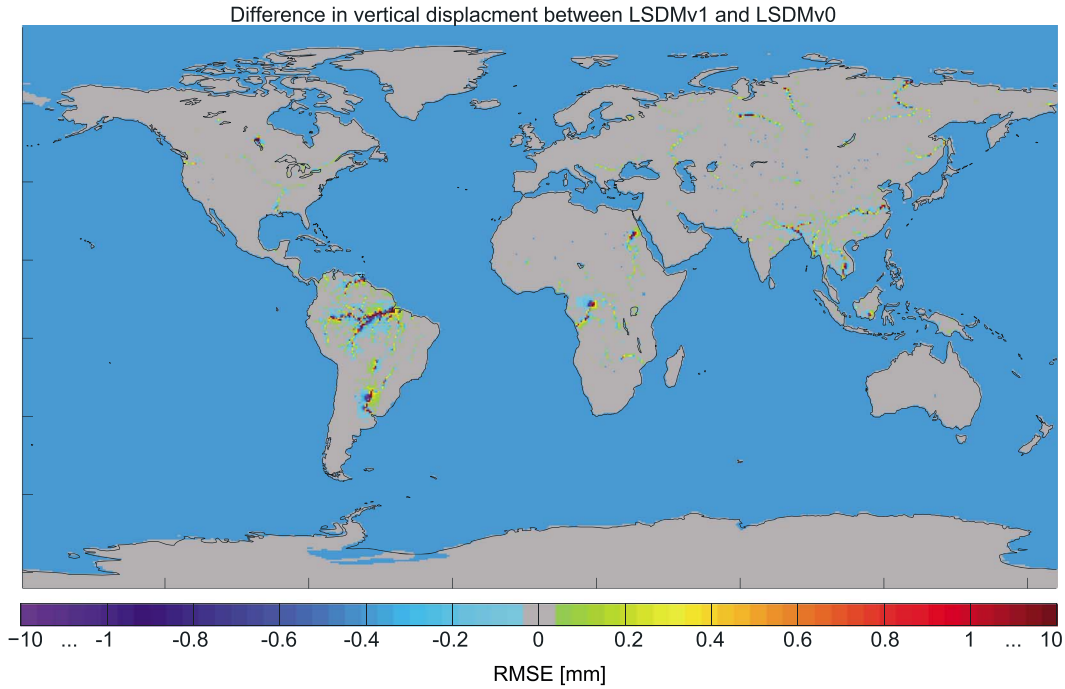

Figure 4. Difference in the RMSE (mm) between LSDMv1 (with river relocation) and LSDMv0 (without river relocation) for the vertical hydrology-induced surface displacements. For better readability the results are masked to the land part; ocean is colored in blue. LSDM = Land Surface Discharge Model; RMSE = root-mean-square error.

network. Generally, we want R_{mg} to prefer the mapping of masses from a single 0.5° grid cells into those 0.125° grid cells that are located inside the 0.5° grid cell area, but sometimes larger sections of rivers need to be distributed as smooth as possible from the artificial model location P_m^l to the geographically more appropriate locations given by P_g^l.

Figure 3 shows exemplary the effect of the relocation procedure for the Yunnan province in southwest China. This region is characterized by many closely located river channels of various length that drain into four different directions. For better demonstration of the river channels, the logarithmic accumulation value instead of the real water height is used as synthetic representation of the river mass stored in the model $M_{0.5}$. The bottom panel of Figure 3 gives the relocated water mass in $G_{0.125}$, again represented as water height. Due to the concentration of the water masses into refined river channels, the water heights are in average 4 times higher. The color gradient of the relocated water storage should follow the color gradient of the original distribution, thereby confirming that the hydrographs are not disturbed. One can identify some stronger accumulations at river junctions, where the relocation procedure is tuned to transfer water preferably into the main river channel instead into its smaller tributaries. This behavior is advantageous as it prevents huge water masses in major river system being falsely mapped into tributary areas with much smaller water storage variations. In other regions, the pairing process identifies several 0.125° grid cells with almost similar matching factors. Consequently, the width of the river channel changes and the water masses are equally distributed into two or more neighboring grid cells. Nevertheless, the hydrograph will be maintained in these areas. However, Figure 3 reveals also some limitations of this automatic generation of the relocation function. In regions with complex alignments of the model rivers with the real river courses further manual editing to obtain a smoother partitioning appears desirable.

Similar to the presented LSDM river network, such a global relocation function can be generated for any other model river network. We obtained reasonable relocation functions also for the 0.5° river network of the WaterGAP Global Hydrology Model (Döll et al., 2003). A test for the river network of the Total Runoff Integrating Pathways river routing model (Oki & Sud, 1998) results in even a slightly more homogeneous relocation function than for the LSDM model. Created once for a specific model river network, the time-invariant relocation function can be applied quickly to the river mass distribution of each model time step.

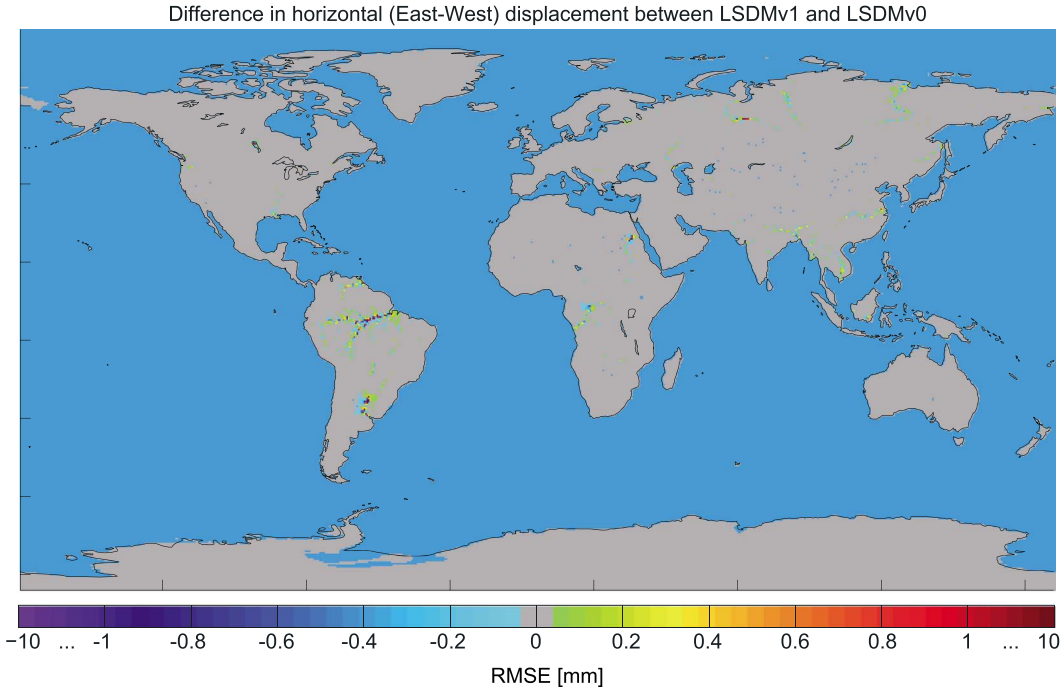

Figure 5. Difference in the RMSE (mm) between LSDMv1 (with river relocation) and LSDMv0 (without river relocation) for the horizontal (east-west) hydrology-induced surface displacements. For better readability the results are masked to the land part; ocean is colored in blue. LSDM = Land Surface Discharge Model; RMSE = root-mean-square error.

3. Calculation of Global-Gridded Surface Deformations

The purpose of the presented relocation procedure is to refine the river mass distribution in order to exploit its full capabilities when calculating global-gridded 0.5° hydrological loading results. The desired spatial

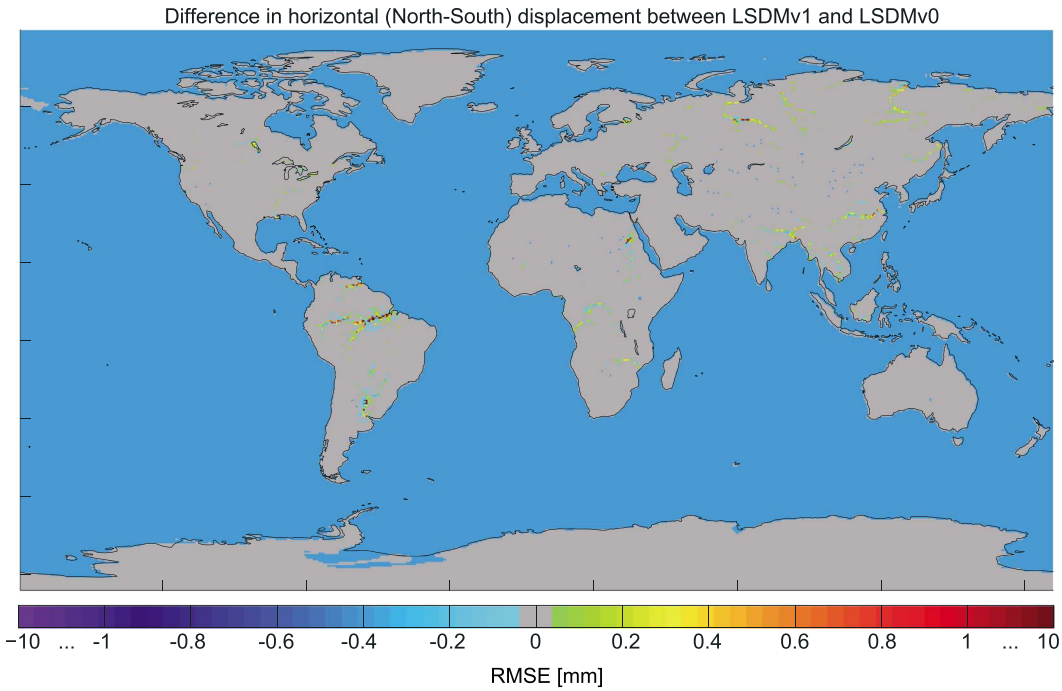

Figure 6. Difference in the RMSE (mm) between LSDMv1 (with river relocation) and LSDMv0 (without river relocation) for the horizontal (north-south) hydrology-induced surface displacements. For better readability the results are masked to the land part; ocean is colored in blue. LSDM = Land Surface Discharge Model; RMSE = root-mean-square error.

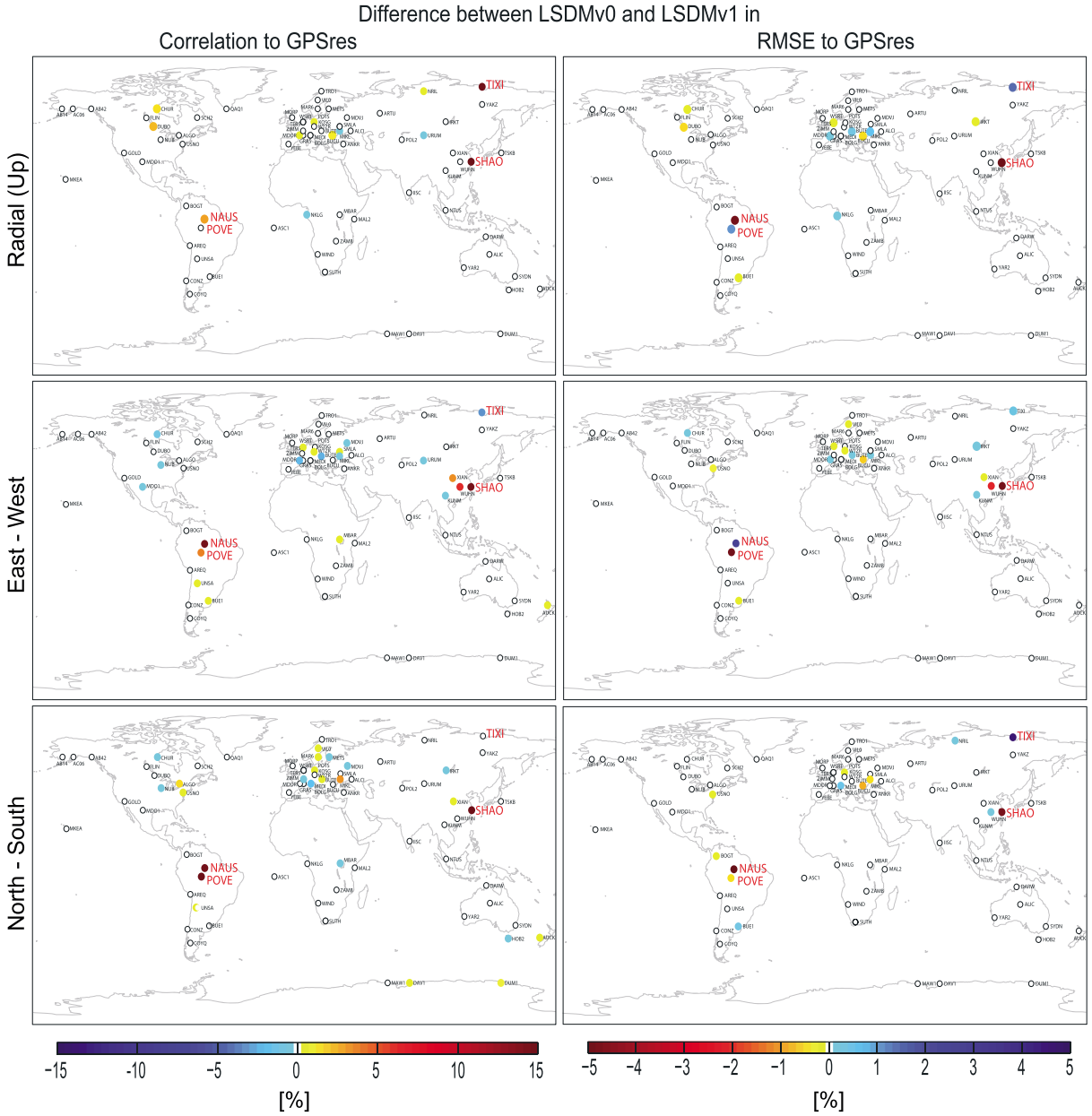

Figure 7. (left column) Difference in correlation between LSDMv1 (with river relocation) and LSDMv0 (without river relocation) with GPS. Positive percentage gives improved correlation of LSDMv1 with GPS compared to LSDMv0. (right column) Difference in RMSE between LSDMv1 and LSDMv0 with GPS. Negative percentage shows improvement of LSDMv1 by a decrease in RMSE compared to RMSE of LSDMv0. LSDM = Land Surface Discharge Model; GPS = Global Positioning System; RMSE = root-mean-square error.

resolution of 0.125° for the modeled water mass load is achieved by separating the 0.5° storage compartments (river and lakes, soil moisture, snow, etc.) of the LSDM simulation, applying the relocation procedure to the river compartment, mapping the water stored in 0.5° lake grid cells homogeneously into related 0.125° lake grid cells, and recombining the new 0.125° river and lake mass distribution with the remaining model compartments interpolated to 0.125°. This refined hydrological mass loads enter the calculation of the elastic Earth surface deformation, based on the fundamental Green's Function approach (Farrell, 1972). At each 0.5° grid point the total surface displacement is the sum of the influence of each 0.125° mass unit, where the influence depends on the amount of mass and its weighting through the Green's function. For the numerical computation we employ the patched Green's function approach (Dill & Dobslaw, 2013) splitting the global convolution into a high-resolution near-field calculation for load distances lower than 3°

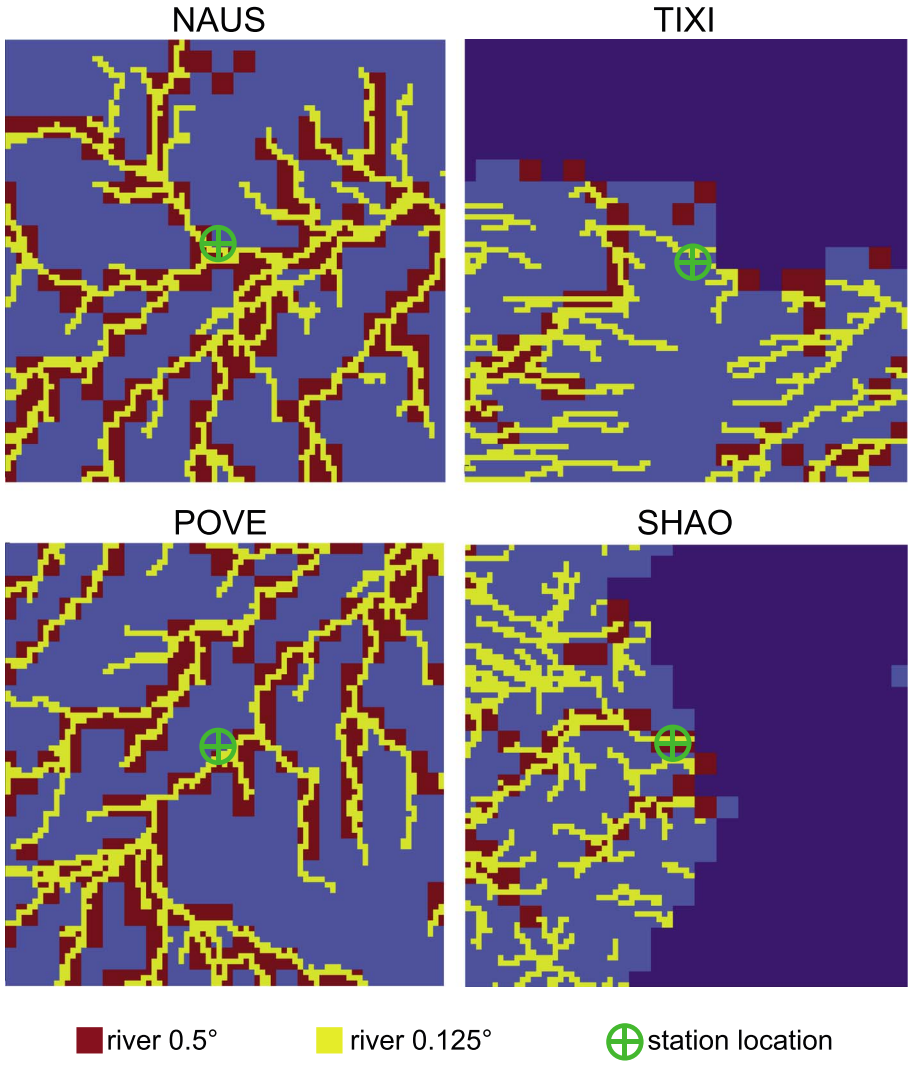

Figure 8. Location of the Global Positioning System stations in Manaus City (NAUS) and Porto Velho (POVE) in the Amazon Basin, Tiksi (TIXI) at Lena River, and Shanghai (SHAO) at Yangtze River. Brown: Land Surface Discharge Model river network; yellow: new 0.125° river map. Note that along the coastline, the rivers are continued into the oceans with one additional ocean cell.

and a low-resolution far-field calculation for larger load distances. The distance-depending Green's functions are calculated from Load Love numbers representing the AK135 Earth model (Kennett et al., 1995), which is a variant of the older IASP91 model (Kennett, 1991). For this study the degree-one deformation is defined for the Earth center of figure reference frame. Individual displacement time series at specific locations of interest are extracted from the global hydrological loading grids by bicubic interpolation, thereby avoiding interpolations across coastlines. GFZ routinely processes such hydrological loading results based on LSDM water mass simulations as operational product for the years 1979 until now available to the public via isdc.gfz-potsdam.de/esmdata/loading. In addition to hydrology-induced surface displacements, consistent loading products for the nontidal atmospheric surface pressure calculated from the European Centre for Medium-Range Weather Forecasts operational numerical weather prediction data and nontidal ocean bottom pressure derived from a general ocean circulation model are utilized to correct GPS observation for those influences.

4. Influence of River Mass Relocation on Hydrological Loading

Figures 4 to 6 give the differences in the root-mean-square error (RMSE) over a 2-year test time span between the results for hydrological loading using LSDM terrestrial water storage including river mass

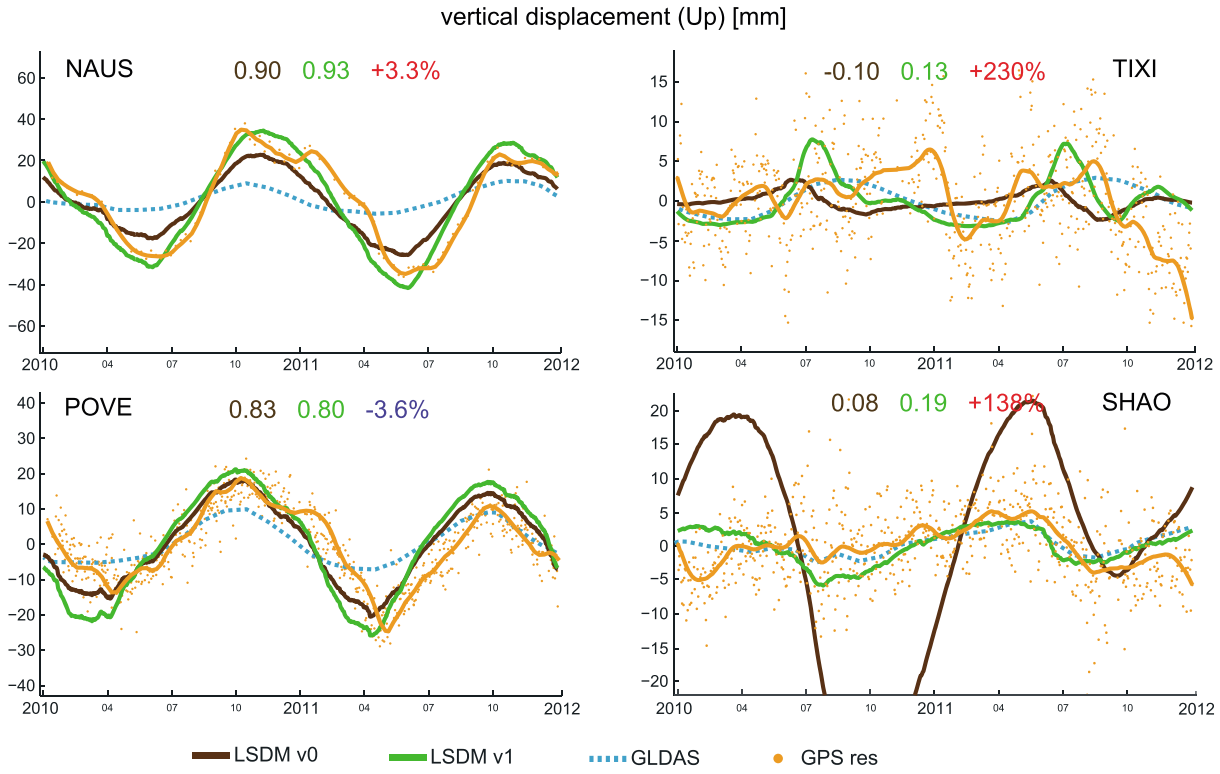

Figure 9. Vertical surface displacement from hydrological models (brown: LSDMv0 without river relocation, green: LSDMv1 with river relocation, dotted blue: GLDAS) and GPS station coordinates (up component) for Manaus City (NAUS) and Porto Velho (POVE) in the Amazon Basin, Tiksi (TIXI) at Lena River, and Shanghai (SHAO) at Yangtze River. Numbers give correlation between GPS and model time series for LSDMv0 (brown), LSDMv1 (green), and relative change (red = improvement / blue = decline). LSDM = Land Surface Discharge Model; GPS = Global Positioning System.

relocation (LSDMv1) and a reference simulation excluding the refinement described above (LSDMv0) for all three components of the surface displacement. As expected, largest differences occur along the main river paths, where the biggest amount of water mass loads enters the relocation procedure. The differences reflect the superposition of two effects when using relocated river masses for hydrology-induced surface displacements. First, the water loads occur at slightly shifted locations, and second, the displacement amplitudes are enhanced due to the concentration of water masses into the 0.125° river channels. Both effects together add up to signed RMSE differences of ±1 mm but can reach −10.2 to +7.4 mm in specific locations like the Amazon Basin, the Winnipeg Lake in Canada, the Nasser Lake at the lower Nile, and along the rivers Parana, Ganges, Yangtze, Ob, and Lena. Although the horizontal displacements are generally smaller than the vertical displacements, the relocation procedure influences the horizontal components with almost the same magnitudes, that is, −1.5 to +3.7 mm (east-west) and −3.2 to +2.7 mm (north-south).

To validate the improvement of the relocation procedure, the simulated crustal deformations are compared to times series of height changes for 75 globally distributed GPS station sites. The GPS time series are downloaded from the data service centers of NASA Jet Propulsion Laboratory (ftp://sideshow.jpl.nasa.gov/pub/JPL_GPS_Timeseries/) and the GPS service for the Geocentric Reference System for the Americas (SIRGAS; ftp://ftp.sirgas.org/pub/gps/SIRGAS). From the weekly GPS time series we removed the estimates of nontidal atmospheric surface pressure loading and nontidal oceanic bottom pressure loading with the help of the data provided by GFZ. The residual signal in the GPS coordinates, denotes as GPSres, is expected to be dominated by hydrology-induced loading in particular at the seasonal period band. Figure 7 shows the correlation (left column) and the RMSE (right column) between LSDMv1 model results and GPS observation, each expressed as percentage relative to the reference LSDMv0 according to

$$C = \frac{\mathrm{corr}(\mathrm{LSDMv1,GPS}) - \mathrm{corr}(\mathrm{LSDMv0,GPS})}{\mathrm{corr}(\mathrm{LSDMv0,GPS})} \times 100 \quad (10)$$

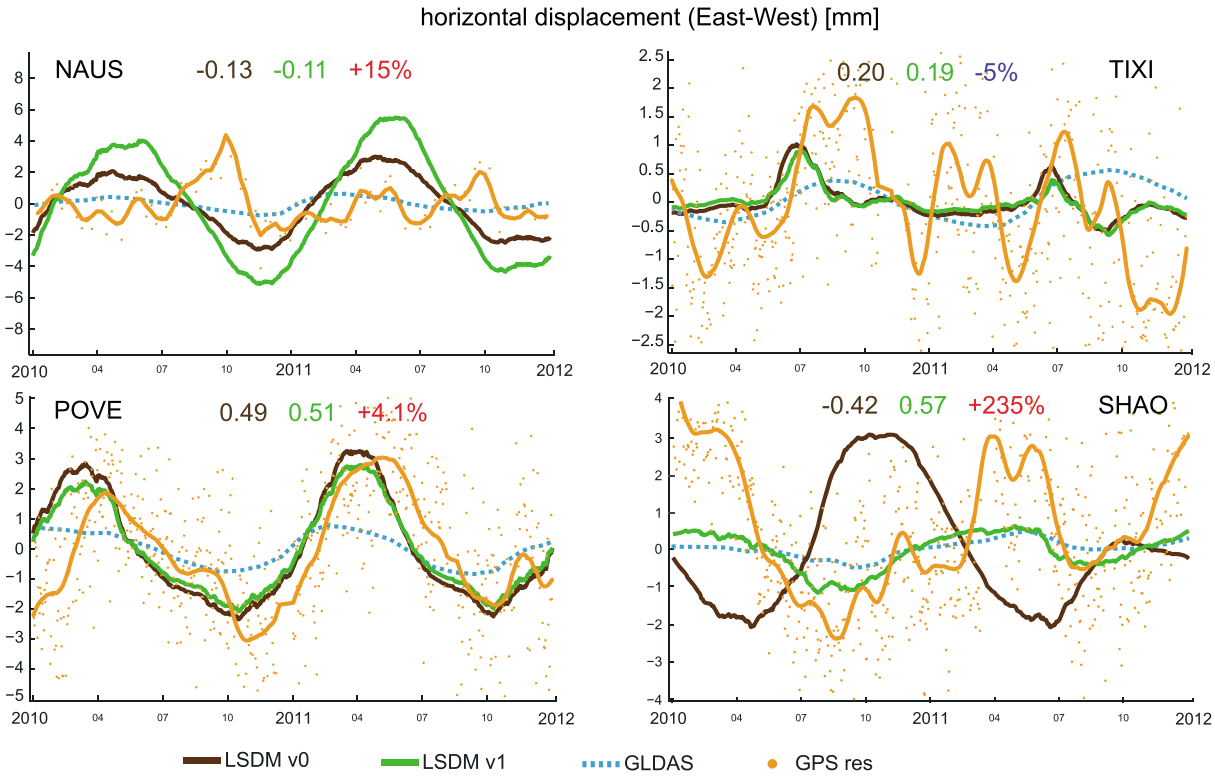

Figure 10. Horizontal east-west surface displacement from hydrological models (brown: LSDMv0 without river relocation, green: LSDMv1 with river relocation, dotted blue: GLDAS) and GPS station coordinates (up component) for Manaus City (NAUS) and Porto Velho (POVE) in the Amazon Basin, Tiksi (TIXI) at Lena River, and Shanghai (SHAO) at Yangtze River. Numbers give correlation between GPS and model time series for LSDMv0 (brown), LSDMv1 (green), and relative change (red = improvement/blue = decline). LSDM = Land Surface Discharge Model; GPS = Global Positioning System.

Colors to the right from yellow to red indicate an improvement (increased correlation, decreased RMSE), and colors to the left from light blue to dark blue indicate a degradation. All stations with significant changes in correlation and/or RMSE are located near major rivers or lakes. Increased correlations indicate a better fit in amplitude, if the time series are in phase, but for out-of-phase time series increased, loading amplitudes lead to decreased correlations. Furthermore, a decrease in correlation could also be a hint that the originally modeled hydrograph has been disturbed by the relocation. Altogether, the small changes in correlation ($< \pm 1\%$) and RMSE ($< \pm 0.5\%$) for most stations underline the robust applicability of the relocation procedure in keeping the modeled hydrographs. The correlation and RMSE changes reveal also a few GPS stations with larger changes. Stations highlighted in red, NAUS, TIXI, POVE, and SHAO, where the most prominent changes occur, are discussed in more detail in Figures 8 to 11.

Station BUCO located in Budapest at the Danube river and DUBO located south of lake Winnipeg in Canada show reduced RMS values, −1%, due to increased seasonal loading amplitudes which fit better to the GPS station measurements. Besides NAUS, POVE, and SHAO also ALGO in the lake area of Canada, MIKL at the river Dnepr between Kiew and the Black Sea, XIAN near the Yellow River, and WUHN at the Yangtze River in China show improved correlations in one or more displacement directions.

The local patterns of the 0.5° model river network (red) and the refined 0.125° river channels (yellow) reveal reasons for the significant changes in the hydrology-induced surface displacement at many of those stations (Figure 8). For NAUS and POVE in the Amazon Basin, the relocation procedure concentrates the river water closer to the station which substantially enhances the loading effect. At TIXI, located in Siberia in the Lena Delta, the hydrological model has a river course through the Lena delta quite different than the river location defined in the 0.125° map. Here the river ends in the Laptev Sea much closer to the station instead of draining further to the north. However, the complex bifurcation of the river channels in the Lena delta is also not resolved in every detail by the relocation and it remains questionable if the 0.5° model water masses could be reasonably distributed in that region with our noninteractive approach. The SHAO station at the Yangtze

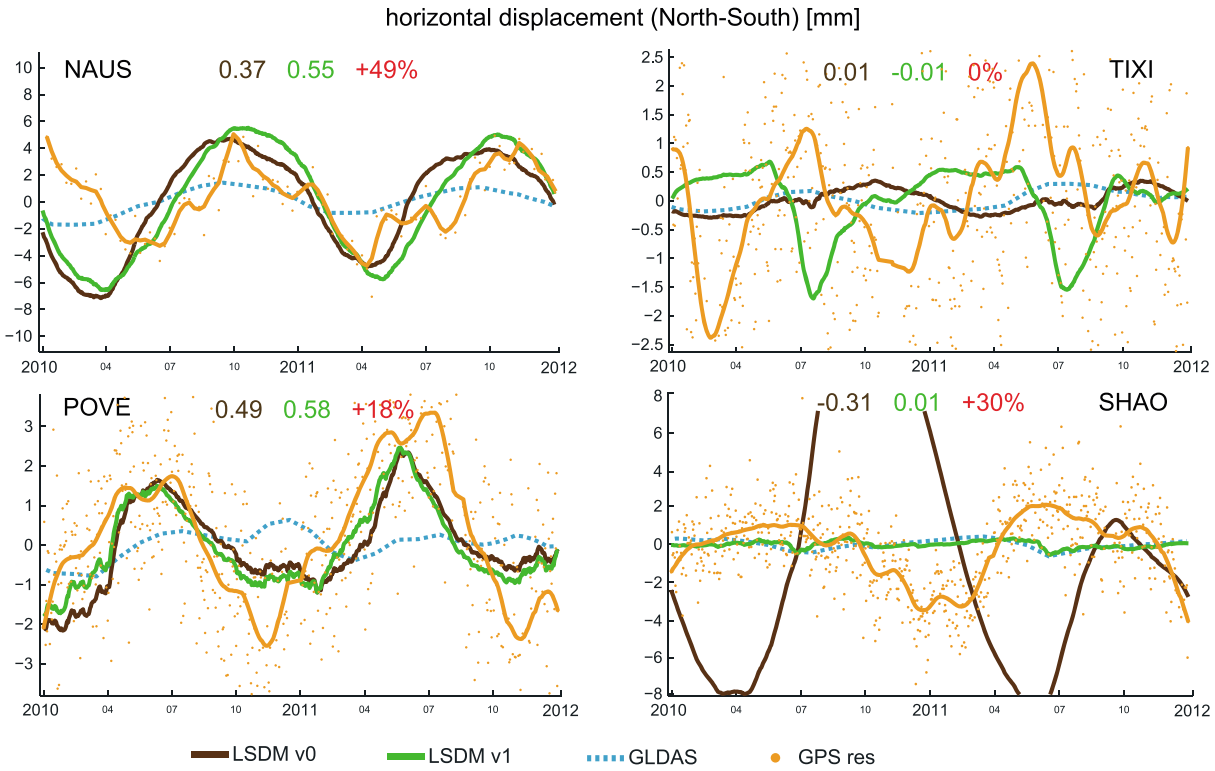

Figure 11. Horizontal north-south surface displacement from hydrological models (brown: LSDMv0 without river relocation, green: LSDMv1 with river relocation, dotted blue: GLDAS) and GPS station coordinates (up component) for Manaus City (NAUS) and Porto Velho (POVE) in the Amazon Basin, Tiksi (TIXI) at Lena River, and Shanghai (SHAO) at Yangtze River. Numbers give correlation between GPS and model time series for LSDMv0 (brown), LSDMv1 (green), and relative change (red = improvement/blue = decline). LSDM = Land Surface Discharge Model; GPS = Global Positioning System.

river in China is located directly in the center of a 0.5° model river grid cell, whereas the relocated river passes the station correctly in the north.

Figures 9 –11 give the individual time series at these four stations for all three displacement components, each comparing the reference calculation LSDMv0, the refined calculation LSDMv1, and the GPS station coordinate residuals. For better visibility, we added a smoothed line calculated by means of a 4-point boxcar filter. Furthermore, time series extracted from the 1.0° hydrological loading product provided by the NASA GSFC Very Large Baseline Interferometry group (Eriksson & MacMillan; http://vlbi.gsfc.nasa.gov/services/hydro_load/) are included. This loading product is based on mass loads from the GLDAS NOAH hydrology model (Rodell et al., 2004) using a lower resolution of monthly 1.0° × 1.0° mass distributions. Differences between the time series clearly highlight the need for denser spatial and temporal resolutions of the river mass loads in order to estimate loading amplitudes correctly in the neighborhood of major rivers.

At NAUS, all three components benefit from the relocation by enhanced amplitudes which fit much better to the GPS observations. At POVE, the GPS observations feature much more scatter. Nevertheless, the vertical component of LSDMv0 correlates already quite well with the GPS time series leading to no further improvement in correlation. RMSE is even slightly degraded as the enhanced amplitudes in LSDMv1 amplify the small phase error existing between LSDMv0 and GPS. The horizontal components show small but significant improvements in correlation and RMSE. Because the river location around TIXI differs completely from the model river network, the modeled vertical component becomes more realistic but still has a low correlation. In the east-west component, changes are marginal, and in the north-south component the amplitudes are larger but, again, with almost no correlation to the GPS results. Both horizontal components suffer from the complex distribution of wetlands and river channels in the Lena delta. At SHAO, the loading time series based on LSDMv0 are clearly overestimated. The reason might be that the station is located inside two 0.5Âř model grid cells that are indicated as swamp region (lakes east of Shanghai) acting like a small reservoir with high retention times. The relocation of the Yangtze River distributes the stored water more realistically along the river channel passing nearby the station location. In consequence LSDMv1 agrees much better to the GPS

time series. Especially in the vertical component, the phase of LSDMv1 is improved, matching now also the phase of the loading results based on GLDAS.

5. Conclusions

The horizontal resolution of global hydrological models is typically limited to 0.5° due to the necessary generalized parametrization of physical processes. In consequence, the models act on a coarse drainage network that is tuned to capture basin-wide characteristics like catchment area, total river length, storage capacity, and retention times correctly on the expense of deviations in the geometry of the river channels. The river locations represented by the model grid cell centers can thus differ significantly from the real location of the rivers. Simulated river flow spreads the water stored in rivers over a sequence of 0.5° grid cells instead of locating the water mass inside the river channels. Using such a model river flow distribution for the calculation of crustal surface displacements results in an underestimation of the hydrology-induced loading signal, especially along the river banks of the world's largest rivers. Modeled surface displacements are improved when calculated from refined water mass distributions that follow closely morphological river channels.

On the basis of high spatial resolution drainage accumulation data from Geo Information Systems, a new 0.125° river map was generated in this study. By automatically classifying associated river parts, a global relocation function was generated that distributes the simulated water masses from the 0.5° model river network into a 0.125° georeferenced river map.

The relocation procedure is applied to the river storage compartment of the global hydrological model LSDM in order to test the impact of such a spatial refinement on hydrology-induced loading calculations. Amplitudes of vertical surface displacements along the major rivers increase by 0.2–5 mm, along the Amazon river even up to additional 15 mm. In the horizontal directions the amplitudes differ up to a maximum of $\pm$3 mm. Due to changes in the river locations, drastic differences in the directions between station position and the loading river mass can significantly affect the horizontal displacement field.

The comparison of modeled displacement time series with GPS station coordinates shows improved correlations and reduced RMSEs for station locations near to major rivers, whereas the matching of modeled loading signals to GPS stations far away from rivers remains almost unchanged.

The presented relocation procedure is able to improve significantly the calculation of hydrology-induced surface displacements. This relocation procedure is, however, not suited to generally refine the output of global hydrological models. The reason is that the partitioning of the coarse model water masses into the refined river grids cannot completely preserve the original model hydrographs. For loading calculations, acting as a spatial low-pass filter, this is instead very well acceptable. In principle, the presented approach allows to define a relocation function for every global hydrological model if the definition of the river network is available and the model provides the output of the river flow and lake compartments separately from all other storage compartments.

Although GRACE observations are an excellent alternative for large-scale modeled terrestrial water storage changes, their use for the calculation of hydrological loading is limited when the dominant wavelength of the load becomes too short (Fu et al., 2013). GRACE-based water masses need a relocation into a refined river network even more than the model-based water masses. Youm et al. (2018) adopted a river routing model to postprocessed and thus strongly smoothed GRACE data. Recursively, they distributed the observed mass in the Amazon Basin along the river channels and obtained a promising agreement between calculated crustal displacements and GPS. However, so far they demonstrated their approach only for one single large catchment. It is also very difficult to separate the water stored in the rivers from the total GRACE observation which includes basically all hydrological storages from water at the surface, soil moisture at different levels, down to the deepest aquifers. Henceforth, a hybrid method taking the information from the model hydrographs, GRACE total water storage, and a high-resolution river map into account together might further improve the correlation of estimated and observed hydrology-induced crustal displacements. Refined hydrological loading results are necessary to remove hydrology-induced displacements from GPS observations to uncover small tectonic signals in the millimeter level, acting, for example, along the Red River Fault in the Yunnan province, China (Zhan et al., 2017). Loading signals induce also aliasing effects in GPS reference frame parameters (Collilieux et al., 2010, 2012). High-resolution hydrological loading can attenuate systematic loading effects caused by nonlinear station motions, especially when the GPS network is not well

distributed and stations near large rivers are involved. The model data provided by GFZ for load-induced surface displacements due to nontidal mass variability in atmosphere, oceans, and terrestrial hydrosphere (isdc.gfz-potsdam.de/esmdata/loading) might be a useful tool for the future research along those directions.

Acknowledgments
Deutscher Wetterdienst, Offenbach, Germany, and the European Centre for Medium-Range Weather Forecasts are acknowledged for providing data from ECMWF's operational model. Numerical simulations were performed at Deutsches Klimarechenzentrum DKRZ, Hamburg, Germany. The operationally updated geophysical loading time series provided by GFZ Potsdam are publicly available at http://isdc.gfz-potsdam.de/esmdata/loading. GPS station position time series are provided by SIRGAS via ftp://ftp.sirgas.org/pub/gps/SIRGAS and UNAVCO at ftp://data-out.unavco.org/pub/products/provision.

References

Bevis, M. (2005). Seasonal fluctuations in the mass of the Amazon River system and Earth's elastic response. *Geophysical Research Letters*, *32*, L16308. https://doi.org/10.1029/2005GL023491

Collilieux, X., Altamimi, Z., Coulot, D., van Dam, T., & Ray, J. (2010). Impact of loading effects on determination of the international terrestrial reference frame. *Advances in Space Research*, *45*(1), 144–154. https://doi.org/10.1016/j.asr.2009.08.024

Collilieux, X., Rebischung, P., van Dam, T., Ray, J., & Altamimi, Z. (2011). Consistency of crustal loading signals derived from models and GPS: A re-examination. In *AGU Fall Meeting Abstracts*. https//adsabs.harvard.edu/abs/2011AGUFM.G31C..01C

Collilieux, X., van Dam, T., Ray, J., Coulot, D., Métivier, L., & Altamimi, Z. (2012). Strategies to mitigate aliasing of loading signals while estimating GPS frame parameters. 1–14. https://doi.org/10.1007/s00190-011-0487-6

Dill, R. (2008). Hydological model LSDM for operational Earth rotation and gravity field variations (*Scientific Technical Report, STR08/09*). Potsdam, Germany: GFZ. 35p.

Dill, R., & Dobslaw, H. (2013). Numerical simulations of global-scale high-resolution hydrological crustal deformations. *Journal of Geophysical Research: Solid Earth*, *118*, 5008–5017. https://doi.org/10.1002/jgrb.50353

Dill, R., Klemann, V., Martinec, Z., & Tesauro, M. (2015). Applying local Green's functions to study the influence of the crustal structure on hydrological loading displacements. *Journal of Geodynamics*, *88*, 14–22. https://doi.org/10.1016/j.jog.2015.04.005

Döll, P., Kaspar, F., & Lehner, B. (2003). A global hydrological model for deriving water availability indicators: Model tuning and validation. *Journal of Hydrology*, *270*, 105–134.

Farrell, W. E. (1972). Deformation of the Earth by surface loads. *Reviews of Geophysics*, *10*, 751–797.

Fritsche, M., Döll, P., & Dietrich, R. (2012). Global-scale validation of model-based load deformation of the Earth's crust from continental watermass and atmospheric pressure variations using GPS. *Journal of Geodynamics*, *59-60*, 133–142.

Fu, Y., Argus, D. F., Freymueller, J. T., & Heflin, M. B. (2013). Horizontal motion in elastic response to seasonal loading of rain water in the Amazon Basin and monsoon water in Southeast Asia observed by GPS and inferred from GRACE. *Geophysical Research Letters*, *40*, 6048–6053. https://doi.org/10.1002/2013GL058093

Fu, Y., Freymueller, J. T., & Jensen, T. (2012). Seasonal hydrological loading in southern Alaska observed by GPS and GRACE. *Geophysical Research Letters*, *39*, L15310. https://doi.org/10.1029/2012GL052453

Jiang, W., Li, Z., van Dam, T., & Ding, W. (2013). Comparative analysis of different environmental loading methods and their impacts on the GPS height time series. *Journal of Geodesy*, *87*, 687–703. https://doi.org/10.1007/s00190-013-0642-3

Kennett, B. L. N. (1991). IASPEI 1991 seismological tables. In *Bibliotech* (p. 167). Canberra, Australia. https://onlinelibrary.wiley.com/doi/epdf/10.1111/j.1365-3121.1991.tb00863.x

Kennett, B. L. N., Engdahl, E. R., & Buland, R. (1995). Constraints on seismic velocities in the Earth from travel times. *Geophysical Journal International*, *122*, 108–124.

Kisseler, A. (2010). Generierung eines globalen Abflussnetzwerkes: GIS-gestützte Präprozessierung für ein globales Abflussmodell am Beispiel des LAnd Surface Discharge Model (LSDM), Magisterarbeit, Universität Freiburg, Institut für Physische Geographie.

Lehner, B., Verdin, K., & Jarvis, A. (2006). *HydroSHEDS Technical Documentation, Version 1.0* (pp. 1–27). Washington, DC: World Wildlife Fund US.

Maidment, D. R. (1996). GIS and hydrological modeling: An assessment of progress. In *Presented at the Third International Conference on GIS and Environmental Modeling*, Santa Fe, New Mexico, pp. 20–25.

Oki, T., & Sud, Y. C. (1998). Design of Total Runoff Integrating Pathways (TRIP)—A global river channel network. *Earth Interactions*, *2*, 1–37. https://doi.org/10.1175/1087-3562(1998)002<0001:DOTRIP>2.3.CO;2

Petrov, L., & Boy, J.-P. (2004). Study of the atmospheric pressure loading signal in VLBI observations. *Journal of Geophysical Research*, *109*, B03405. https://doi.org/10.1029/2003JB002500

Rajner, M., & Liwosz, T. (2011). Studies of crustal deformation due to hydrological loading on GPS height estimates. *Geodesy and Cartography*, *60*, 135–144. https://doi.org/10.2478/v10277-012-0012-y

Rodell, M., Houser, P. R., Jambor, U., Gottschalck, J., Mitchell, K., Meng, C.-J., et al. (2004). The global land data assimilation system. *Bulletin of the American Meteorological Society*, *85*, 381–394. https://doi.org/10.1175/BAMS-85-3-381

Tregoning, P., Watson, C., & Ramillien, G. (2009). Detecting hydrologic deformation using GRACE and GPS. *Geophysical Research Letters*, *36*, L15401. https://doi.org/10.1029/2009GL038718

Wesseling, C. G., Van Deursen, W. P. A., & De Wit, M. (1997). Large scale catchment delineation: A case study for the river Rhine Basin. *Geographical Information*, *1*, 487–496. Joint European conference; 3rd, Geographical information.

Williams, S. D. P., & Penna, N. T. (2011). Non-tidal ocean loading effects on geodetic GPS heights. *Geophysical Research Letters*, *38*, L09314. https://doi.org/10.1029/2011GL046940

Youm, K., Eom, J., & Seo, K. (2018). Crustal displacement in Amazon River basin using GRACE and a river routing model. *Presentation at EGU General Assembley 2018, Vienna*. https//meetingorganizer.copernicus.org/EGU2018/EGU2018-16351.pdf

Zhan, W., Li, F., Hao, W., & Yan, J. (2017). Regional characteristics and influencing factors of seasonal vertical crustal motions in Yunnan, China. *Geophysical Journal International*, *210*(3), 1295–1304. https://doi.org/10.1093/gji/ggx246